

Observation of the doubly Cabibbo-suppressed decays $D^+ \rightarrow K^+ \pi^0 \pi^0$ and $D^+ \rightarrow K^+ \pi^0 \eta$



The BESIII collaboration

E-mail: besiii-publications@ihep.ac.cn

ABSTRACT: By analyzing e^+e^- annihilation data corresponding to an integrated luminosity of 2.93 fb^{-1} collected at the center-of-mass energy of 3.773 GeV with the BESIII detector, we report the first observations of the doubly Cabibbo-suppressed decays $D^+ \rightarrow K^+ \pi^0 \pi^0$ and $D^+ \rightarrow K^+ \pi^0 \eta$. The branching fractions of $D^+ \rightarrow K^+ \pi^0 \pi^0$ and $D^+ \rightarrow K^+ \pi^0 \eta$ are measured to be $(2.1 \pm 0.4_{\text{stat}} \pm 0.1_{\text{syst}}) \times 10^{-4}$ and $(2.1 \pm 0.5_{\text{stat}} \pm 0.1_{\text{syst}}) \times 10^{-4}$ with statistical significances of 8.8σ and 5.5σ , respectively. In addition, we search for the subprocesses $D^+ \rightarrow K^*(892)^+ \pi^0$ and $D^+ \rightarrow K^*(892)^+ \eta$ with $K^*(892)^+ \rightarrow K^+ \pi^0$. The branching fraction of $D^+ \rightarrow K^*(892)^+ \eta$ is determined to be $(4.4_{-1.5}^{+1.8}_{\text{stat}} \pm 0.2_{\text{syst}}) \times 10^{-4}$, with a statistical significance of 3.2σ . No significant signal for $D^+ \rightarrow K^*(892)^+ \pi^0$ is found and we set an upper limit on the branching fraction of this decay at the 90% confidence level to be 5.4×10^{-4} .

KEYWORDS: Branching fraction, Charm Physics, e^+e^- Experiments, Flavour Physics

ARXIV EPRINT: [2110.10999](https://arxiv.org/abs/2110.10999)

Contents

1	Introduction	1
2	BESIII detector and Monte Carlo simulation	2
3	Measurement method and single tag yields	2
4	Yields of double-tag events	3
5	Systematic uncertainty	6
6	Summary	9
The BESIII collaboration		14

1 Introduction

Hadronic D decays open an important window to explore weak D decay mechanisms. Based on quark SU(3)-flavor symmetry, the branching fractions (BFs) of two-body hadronic $D \rightarrow VP$ decays, where V and P denote vector and pseudoscalar mesons, respectively, have been calculated with various approaches [1–3]. The effect of quark SU(3)-flavor symmetry breaking has been validated in Cabibbo-favored (CF) and singly Cabibbo-suppressed $D \rightarrow VP$ decays. However, experimental information related to doubly Cabibbo-suppressed (DCS) $D \rightarrow VP$ decays is rare, due to their small BFs coupled with large backgrounds. The BFs of the DCS decays $D^+ \rightarrow K^{*+}\pi^0$ and $D^+ \rightarrow K^{*+}\eta$ are predicted to be $\sim 10^{-4}$, and the ratio of these branching ratios $\frac{\mathcal{B}_{D^+ \rightarrow K^{*+}\pi^0}}{\mathcal{B}_{D^+ \rightarrow K^{*+}\eta}}$ is estimated to be either 2.86 ± 0.76 [1] or 4 [2]. Improved understanding of U-spin and SU(3)-flavor symmetry breaking effects can be derived from these decays, which can lead to more precise theoretical predictions of CP violation in the charm sector [1–8].

Unlike the DCS decay $D^+ \rightarrow K^0\pi^+\pi^0$, which has a large irreducible background from the CF decay $D^+ \rightarrow \bar{K}^0\pi^+\pi^0$, the $D^+ \rightarrow K^+\pi^0\pi^0$ decay offers a unique low-background opportunity to investigate $D^+ \rightarrow K^{*+}\pi^0$ with $K^{*+} \rightarrow K^+\pi^0$ decay. A similar argument can be made to study $D^+ \rightarrow K^+\pi^0\eta$ decays. Isospin statistical models indicate that the BF of $D^+ \rightarrow K^+\pi^0\pi^0$ is one-third of that of $D^+ \rightarrow K^+\pi^+\pi^-$ [11, 12]. Since the BF of the DCS decay $D^+ \rightarrow K^+\pi^+\pi^-$ relative to its CF counterpart $D^+ \rightarrow K^-\pi^+\pi^+$ is naively expected to be about $2 \tan^4 \theta_C$ [13], where $\tan^4 \theta_C = 0.29\%$ and θ_C is the Cabibbo mixing angle [9, 10], the ratio $\frac{\mathcal{B}_{D^+ \rightarrow K^+\pi^0\pi^0}}{\mathcal{B}_{D^+ \rightarrow K^-\pi^+\pi^+}}$ is expected to be $\frac{2}{3} \tan^4 \theta_C$. Therefore, experimental studies of $D^+ \rightarrow K^+\pi^0\pi^0$ and $D^+ \rightarrow K^+\pi^0\eta$ decays provide a powerful way to further understand the decay dynamics of charmed mesons. Throughout the text, charge conjugated decays are always implied and K^{*+} denotes the $K^*(892)^+$, which has a mass of $0.892 \text{ GeV}/c^2$ [13].

This paper reports the first experimental studies of $D^+ \rightarrow K^+\pi^0\pi^0$, $D^+ \rightarrow K^+\pi^0\eta$, $D^+ \rightarrow K^{*+}\pi^0$, and $D^+ \rightarrow K^{*+}\eta$. This analysis uses a sample of e^+e^- annihilation data [14, 15] taken with the BESIII detector at the center-of-mass energy $\sqrt{s} = 3.773$ GeV. This energy point is above the threshold to produce $D\bar{D}$ and below that to produce $D^*\bar{D}$, where D and D^* denote charged or neutral charmed meson and their excited states, respectively. Therefore, the D and \bar{D} mesons are produced exclusively in pairs, with no additional hadrons accompanying them. This sample corresponds to an integrated luminosity of 2.93 fb^{-1} .

2 BESIII detector and Monte Carlo simulation

The BESIII detector is a magnetic spectrometer [17] located at the Beijing Electron Positron Collider (BEPCII) [16]. The cylindrical core of the BESIII detector consists of a helium-based multilayer drift chamber, a plastic scintillator time-of-flight system (TOF), and a CsI (Tl) electromagnetic calorimeter (EMC), which are all enclosed in a superconducting solenoidal magnet providing a 1.0 T magnetic field. The solenoid is supported by an octagonal flux-return yoke with resistive-plate counter muon-identifier modules interleaved with steel. The acceptance of charged particles and photons is 93% over 4π solid angle. The charged-particle momentum resolution at 1 GeV/ c is 0.5%, and the resolution of the specific ionization energy loss is 6% for the electrons from Bhabha scattering. The EMC measures photon energies with a resolution of 2.5% (5%) at 1 GeV in the barrel (end cap) region. The time resolution of the TOF barrel part is 68 ps, while that of the end cap part is 110 ps.

Details about the design and performance of the BESIII detector are given in refs. [17]. Simulated samples produced with a GEANT4-based [18–20] Monte Carlo (MC) simulation, which includes the geometric description of the BESIII detector and the detector response, are used to determine the detection efficiency and to estimate backgrounds. The simulation includes the beam energy spread and initial state radiation (ISR) in the e^+e^- annihilations modeled with the generator KKMC [21, 22]. The signal of $D^+ \rightarrow K^+\pi^0\pi^0(\eta)$ is simulated using an MC generator that incorporates the resonant decay $D^+ \rightarrow K^{*+}\pi^0(\eta)$ and the phase space decay $D^+ \rightarrow K^+\pi^0\pi^0(\eta)$. The background is studied using an inclusive MC sample that consists of the production of $D\bar{D}$ pairs with consideration of quantum coherence for all neutral D modes, the non- $D\bar{D}$ decays of the $\psi(3770)$, the ISR production of the J/ψ and $\psi(3686)$ states, and the continuum processes incorporated in KKMC [21, 22]. The known decay modes are modeled with EVTGEN [23, 24] using the corresponding BFs taken from the Particle Data Group [13], while the remaining unknown decays from the charmonium states are modeled with LUNDCHARM [25, 26]. Final state radiation from charged final state particles is incorporated using PHOTOS [27–29].

3 Measurement method and single tag yields

The BFs of the signal decays are measured with a double-tag (DT) technique that was first developed by the Mark III Collaboration [30]. The signal D^+ decays are reconstructed

alongside hadronic D^- decays to $K^+\pi^-\pi^-$, $K_S^0\pi^-$ and $K^+\pi^-\pi^-\pi^0$. This tag combination is chosen from the six widely-used D^- tag modes of $D^- \rightarrow K^+\pi^-\pi^-$, $K_S^0\pi^-$, $K^+\pi^-\pi^-\pi^0$, $K_S^0\pi^-\pi^0$, $K_S^0\pi^+\pi^-\pi^-$ and $K^+K^-\pi^-$ in most studies of D^+ decays, based on the optimization of the figure of merit $S/\sqrt{S+B}$. Here, S is the signal yield expected based on the known BF of $D^+ \rightarrow K^+\pi^+\pi^-$ or $D^+ \rightarrow K_S^0\pi^+\eta$, which are isospin symmetric decays of the DCS decays of interest; and B is the scaled background yield estimated by the inclusive MC sample. The fully reconstructed D^- is called the single-tag (ST) meson. Events in which both the signal D^+ meson and the ST D^- meson are found are called DT events. For a given signal decay, the decay BF is determined by

$$\mathcal{B}_{\text{sig}} = N_{\text{DT}} / (N_{\text{ST}} \cdot \epsilon_{\text{sig}} \cdot \mathcal{B}_{\text{sub}}), \tag{3.1}$$

where N_{ST} and N_{DT} are the yields of ST and DT candidates in data, $\epsilon_{\text{sig}} = \sum_{i=1}^3 [(N_{\text{ST}}^i \cdot \epsilon_{\text{DT}}^i) / (N_{\text{ST}} \cdot \epsilon_{\text{ST}}^i)]$ is the signal efficiency in the presence of the ST candidate, in which ϵ_{ST} and ϵ_{DT} are the efficiencies of selecting ST and DT candidates, and i stands for tag modes. The \mathcal{B}_{sub} is the product of BF of the subdecays of K^{*+} , π^0 and η .

Candidate K_S^0 , π^0 , and η mesons are formed via the decays $K_S^0 \rightarrow \pi^+\pi^-$, $\pi^0 \rightarrow \gamma\gamma$, and $\eta \rightarrow \gamma\gamma$. The K^\pm , π^\pm , K_S^0 , π^0 , and η candidates are reconstructed and identified using the same criteria as in refs. [31, 32].

The ST D^- mesons are distinguished from combinatorial background using two kinematic variables: the energy difference $\Delta E_{\text{tag}} \equiv E_{D^-} - E_{\text{b}}$ and the beam-constrained mass $M_{\text{BC}}^{\text{tag}} \equiv \sqrt{E_{\text{b}}^2 - |\vec{p}_{D^-}|^2}$. Here, E_{b} is the beam energy, and \vec{p}_{D^-} and E_{D^-} are the momentum and energy, respectively, of the D^- candidate in the rest frame of the e^+e^- system. If more than one candidate survives the selection criteria of a given tag mode, the combination with the minimum $|\Delta E_{\text{tag}}|$ is chosen. Tagged D^- candidates are selected with a requirement of $\Delta E_{\text{tag}} \in (-25, 25)$ MeV for the decay modes $D^- \rightarrow K^+\pi^-\pi^-$ and $D^- \rightarrow K_S^0\pi^-$; and $\Delta E_{\text{tag}} \in (-55, 40)$ MeV for $D^- \rightarrow K^+\pi^-\pi^-\pi^0$ to suppress combinatorial backgrounds in the $M_{\text{BC}}^{\text{tag}}$ distributions. To extract the number of ST D^- mesons for each tag mode, maximum likelihood fits have been performed on the individual $M_{\text{BC}}^{\text{tag}}$ distributions [31, 32]. The ST yields and efficiencies for various tag modes are summarized in table 1. The number of ST D^- mesons summed over the three tag modes is $N_{\text{ST}} = (1150.3 \pm 1.5_{\text{stat}}) \times 10^3$.

4 Yields of double-tag events

Candidates for the DCS D^+ decays are selected with the residual neutral and charged particles not used in the D^- tag reconstruction. Similar to the tag side, the energy difference and beam-constrained mass of the signal side, ΔE_{sig} and $M_{\text{BC}}^{\text{sig}}$, respectively, are calculated. For each signal decay, if there are multiple combinations, the one giving the minimum $|\Delta E_{\text{sig}}|$ is kept. The accepted candidates are required to fall in the intervals $\Delta E_{\text{sig}} \in (-78, 36)$ MeV and $\Delta E_{\text{sig}} \in (-52, 31)$ MeV for $D^+ \rightarrow K^+\pi^0\pi^0$ and $D^+ \rightarrow K^+\pi^0\eta$, respectively. To reduce background events from non- D^+D^- processes, the minimum opening angle between the D^+ and D^- must be greater than 167° . This requirement suppresses

57% (81%) of background for $D^+ \rightarrow K^+\pi^0\pi^0(\eta)$ at the cost of losing 9% of the two signal decays. For $D^+ \rightarrow K^+\pi^0\pi^0$, the invariant mass of the $\pi^0\pi^0$ combination is required to be outside $(0.388, 0.588) \text{ GeV}/c^2$ to reject the dominant background from the singly Cabibbo-suppressed decay $D^+ \rightarrow K^+K_S^0(\rightarrow \pi^0\pi^0)$.

The resulting distributions of $M_{\text{BC}}^{\text{tag}}$ versus $M_{\text{BC}}^{\text{sig}}$ of the accepted DT candidates are shown in the left column of figure 1. Signal events cluster around $M_{\text{BC}}^{\text{tag}} = M_{\text{BC}}^{\text{sig}} = M_{D^+}$, where M_{D^+} is the known D^+ mass [13]. There are three kinds of background events. The events with correctly reconstructed D^+ (D^-) and incorrectly reconstructed D^- (D^+) are called BKGI. These background events are distributed along the horizontal and vertical bands around the known D^+ mass. The events spreading along the diagonal, which are mainly from the $e^+e^- \rightarrow q\bar{q}$ processes, are named BKGII. The events with incorrectly reconstructed D^- and D^+ are dispersed in the allowed kinematic region and they are ignored in the following analysis due to limited statistics.

The signal yields of the DT events are extracted from a two-dimensional (2D) unbinned maximum likelihood fit to the corresponding distribution of $M_{\text{BC}}^{\text{tag}}$ versus $M_{\text{BC}}^{\text{sig}}$. The signal shape is described by the 2D probability density function (PDF) from the MC simulation after convolving with a Gaussian resolution function with parameters derived from the control sample of $D^+ \rightarrow \pi^+\pi^0\pi^0$. For various background components, the individual PDFs are constructed as [32, 33]

- BKGI: $b(x) \cdot c_y(y; E_b, \xi_y) + b(y) \cdot c_x(x; E_b, \xi_x)$,
- BKGII: $c_z(z; \sqrt{2}E_b, \xi_z) \cdot g(k; 0, \sigma_k)$,

Here, $x = M_{\text{BC}}^{\text{tag}}$, $y = M_{\text{BC}}^{\text{sig}}$, $z = (x + y)/\sqrt{2}$, and $k = (x - y)/\sqrt{2}$. The one-dimensional MC-simulated signal shapes are $b(x)$ and $b(y)$. The c_f is an ARGUS function [34] defined as

$$c_f(f; E_{\text{end}}, \xi_f) = A_f \cdot f \left(1 - \frac{f^2}{E_{\text{end}}^2} \right)^{\frac{1}{2}} \cdot e^{-\xi_f \cdot \left(1 - \frac{f^2}{E_{\text{end}}^2} \right)}, \quad (4.1)$$

where $f \equiv x, y$, or z , A_f is a normalization factor, ξ_f is a fit parameter, and E_{end} is the endpoint fixed at E_b for c_x and c_y or $\sqrt{2}E_b$ for c_z . The function $g(k; 0, \sigma_k)$ is a Gaussian function with zero mean and standard deviation $\sigma_k = \sigma_0 \cdot (\sqrt{2}E_b - z)^p$, where σ_0 and p are the parameters determined from the fit. The weights of $b(x) \cdot c_y(y; E_b, \xi_y)$ and $b(y) \cdot c_x(x; E_b, \xi_x)$ are absorbed by normalization factor A_f . All other parameters are free in the fit. The spectra of the middle and right columns in figure 1 show the projections on $M_{\text{BC}}^{\text{tag}}$ and $M_{\text{BC}}^{\text{sig}}$ of the 2D fits to data. These fits give the signal yields of $D^+ \rightarrow K^+\pi^0\pi^0$ and $D^+ \rightarrow K^+\pi^0\eta$ to be $42.8 \pm 7.2_{\text{stat}}$ and $19.2 \pm 5.0_{\text{stat}}$, respectively.

To account for the large difference of detection efficiencies between resonant and non-resonant decays, we estimate the resonant component of $D^+ \rightarrow K^{*+}\pi^0(\eta)$ under the assumption that the non-resonant component is uniformly distributed and there is no interference between the two kinds of components. The signal yield of the resonant decay $D^+ \rightarrow K^{*+}\pi^0(\eta)$ is extracted from a simultaneous 2D fit in the K^{*+} signal and sideband regions.

The K^{*+} signal region is defined as the invariant mass $M_{K^+\pi^0} \in (0.792, 0.992) \text{ GeV}/c^2$ for $D^+ \rightarrow K^{*+}\eta$ and one of two $M_{K^+\pi^0}$ combinations lying in $M_{K^+\pi^0} \in$

Tag mode i	$D^- \rightarrow K^+\pi^-\pi^-$	$D^- \rightarrow K_S^0\pi^-$	$D^- \rightarrow K^+\pi^-\pi^-\pi^0$	Average
N_{ST}^i	798935 ± 1011	93308 ± 329	258044 ± 1036	...
ϵ_{tag}^i	0.5190 ± 0.0008	0.5180 ± 0.0017	0.2692 ± 0.0009	...
$\epsilon_{\text{tag}, D^+ \rightarrow K^+\pi^0\pi^0}^i$	0.0966 ± 0.0001	0.1004 ± 0.0003	0.0429 ± 0.0001	...
$\epsilon_{D^+ \rightarrow K^+\pi^0\pi^0}^i$	0.1862 ± 0.0003	0.1937 ± 0.0008	0.1595 ± 0.0006	0.1808 ± 0.0003
$\epsilon_{\text{tag}, D^+ \rightarrow K^{*+}\pi^0}^i$	0.0697 ± 0.0001	0.0731 ± 0.0003	0.0305 ± 0.0001	...
$\epsilon_{D^+ \rightarrow K^{*+}\pi^0}^i$	0.1344 ± 0.0003	0.1411 ± 0.0008	0.1133 ± 0.0005	0.1302 ± 0.0003
$\epsilon_{\text{tag}, D^+ \rightarrow K^+\pi^0\eta}^i$	0.1093 ± 0.0001	0.1122 ± 0.0003	0.0494 ± 0.0001	...
$\epsilon_{D^+ \rightarrow K^+\pi^0\eta}^i$	0.2105 ± 0.0004	0.2166 ± 0.0009	0.1835 ± 0.0007	0.2050 ± 0.0003
$\epsilon_{\text{tag}, D^+ \rightarrow K^{*+}\eta}^i$	0.0888 ± 0.0002	0.0915 ± 0.0006	0.0395 ± 0.0001	...
$\epsilon_{D^+ \rightarrow K^{*+}\eta}^i$	0.1710 ± 0.0005	0.1769 ± 0.0012	0.1467 ± 0.0006	0.1660 ± 0.0004

Table 1. The ST yields (N_{ST}^i), the ST efficiencies (ϵ_{tag}^i), the DT efficiencies ($\epsilon_{\text{DT}}^i = \epsilon_{\text{tag, sig}}^i$), and the signal efficiencies (ϵ_{sig}^i). Compared to the mixed signal MC events, the lower signal efficiencies for the resonant decays are mainly due to that the π^0 s from K^{*+} decays have much lower momenta and an additional K^{*+} mass requirement. For $D^- \rightarrow K^+\pi^-\pi^-\pi^0$, the efficiencies are lower than those of the other two tag modes, mainly because of more migrations of low momentum pions between tag and signal sides. The efficiencies do not include the BFs of subresonance decays. The uncertainties are statistical only.

(0.792, 0.992) GeV/ c^2 for $D^+ \rightarrow K^{*+}\pi^0$. The sideband region is defined as the $K^+\pi^0$ combination outside the K^{*+} signal region but within the kinematic region. Definitions of the K^{*+} signal and sideband regions are shown in figure 2.

The left columns of figures 3(a) and 3(b) show the $M_{\text{BC}}^{\text{tag}}$ versus $M_{\text{BC}}^{\text{sig}}$ distributions of the accepted DT candidates, where the top and bottom rows correspond to the K^{*+} signal and sideband regions, respectively. In the simultaneous fits, the ratios of the non-resonant background yields between the K^{*+} sideband and signal regions are fixed to the MC-determined values of $f_{K^{*+}\pi^0} = 1.40 \pm 0.02$ for $D^+ \rightarrow K^+\pi^0\pi^0$ and $f_{K^{*+}\eta} = 2.25 \pm 0.05$ for $D^+ \rightarrow K^+\pi^0\eta$, respectively, where the efficiency differences have been considered. In addition, the parameters of the ARGUS functions in the 2D fit to the K^{*+} sideband events are constrained to be the same as those for the K^{*+} signal region. The other parameters are left free. These fits give the signal yields of $D^+ \rightarrow K^{*+}\pi^0$ and $D^+ \rightarrow K^{*+}\eta$ to be $16.6_{-6.2}^{+6.6}_{\text{stat}}$ and $10.9_{-3.8}^{+4.4}_{\text{stat}}$, respectively. Combining the $D^+ \rightarrow K^+\pi^0\pi^0$ and $D^+ \rightarrow K^+\pi^0\eta$ signal yields, we obtain the fractions of the resonant components to be $r_{K^{*+}\pi^0} = 0.39 \pm 0.17_{\text{stat}}$ and $r_{K^{*+}\eta} = 0.57 \pm 0.28_{\text{stat}}$, respectively.

The efficiency of detecting the signal decay $D^+ \rightarrow K^+\pi^0\pi^0(\eta)$ is estimated by using a mixture of the signal MC events for the resonant decay $D^+ \rightarrow K^{*+}\pi^0(\eta)$ and the phase space decay $D^+ \rightarrow K^+\pi^0\pi^0(\eta)$ with fractions of $r_{K^{*+}\pi^0}$ and $r_{K^{*+}\eta}$ determined above. The obtained DT efficiencies ($\epsilon_{\text{DT}}^i = \epsilon_{\text{tag, sig}}^i$) and signal efficiencies (ϵ_{sig}^i) for individual decays are summarized in table 1.

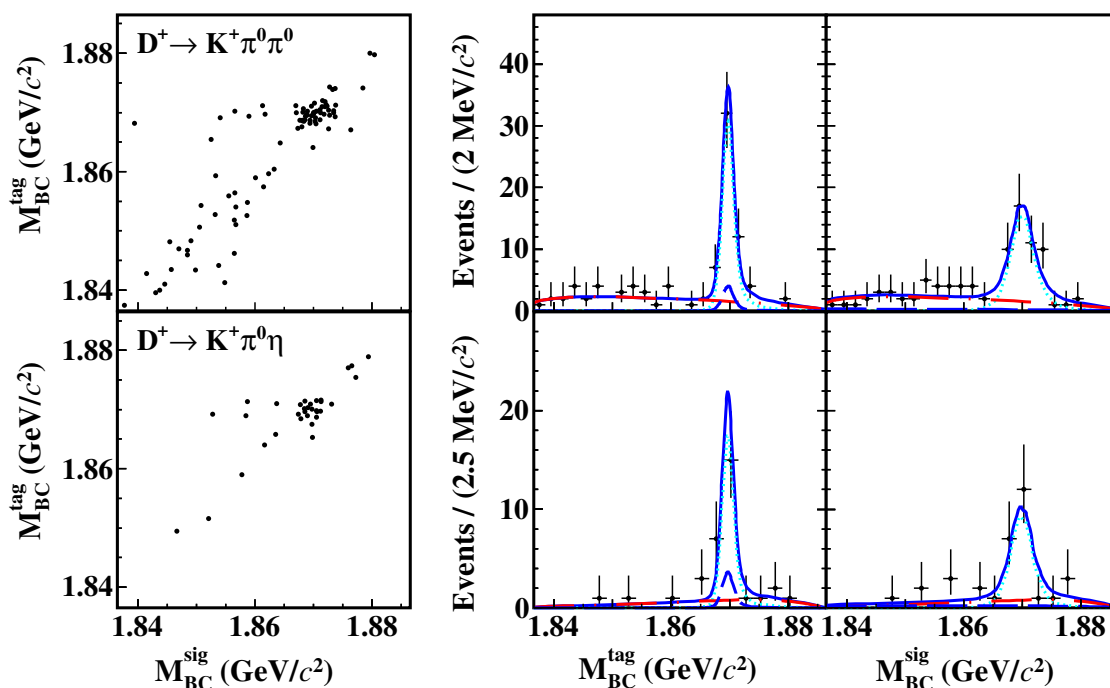


Figure 1. Distributions of (left column) M_{BC}^{tag} versus M_{BC}^{sig} and the projections on (middle column) M_{BC}^{tag} and (right column) M_{BC}^{sig} of the 2D fits to the DT candidate events. The top row is for $D^+ \rightarrow K^+ \pi^0 \pi^0$ and the bottom row is for $D^+ \rightarrow K^+ \pi^0 \eta$. Points with error bars are data. Blue solid curves are the fit results. Cyan dotted curves are the fitted signal distributions. Blue long-dashed curves are BKGI. Red dot-long-dashed curves are BKGI.

For each signal decay, the statistical significance is evaluated using $\sqrt{-2\ln(\mathcal{L}_0/\mathcal{L}_{\text{max}})}$, where \mathcal{L}_{max} is the maximum likelihood of the nominal fit and \mathcal{L}_0 is obtained by refitting the M_{BC}^{tag} versus M_{BC}^{sig} distribution without the signal PDF. Especially, the peaking background of the non-resonant component has been fixed for $D^+ \rightarrow K^{*+} \pi^0$ and $D^+ \rightarrow K^{*+} \eta$. The resulting statistical significances are 8.8σ , 5.5σ , 2.7σ , and 3.2σ for $D^+ \rightarrow K^+ \pi^0 \pi^0$, $D^+ \rightarrow K^+ \pi^0 \eta$, $D^+ \rightarrow K^{*+} \pi^0$, and $D^+ \rightarrow K^{*+} \eta$, respectively. In addition, 10000 toy MC studies show that the 2D fit is stable and no potential bias is found for each signal decay.

The measured values for N_{DT} , ϵ_{sig} , and \mathcal{B}_{sig} are summarized in table 2. Because there is no significant signal for $D^+ \rightarrow K^{*+} \pi^0$, we set an upper limit on its decay BF at the 90% confidence level to be 5.4×10^{-4} . This is set utilizing the Bayesian approach after incorporating the associated systematic uncertainty [35], as discussed later.

5 Systematic uncertainty

One of the advantages of the DT method is that most of the uncertainties associated with the ST selection cancel. The systematic uncertainties in the BF measurements are mainly from the following sources. They are reported relative to the measured BFs.

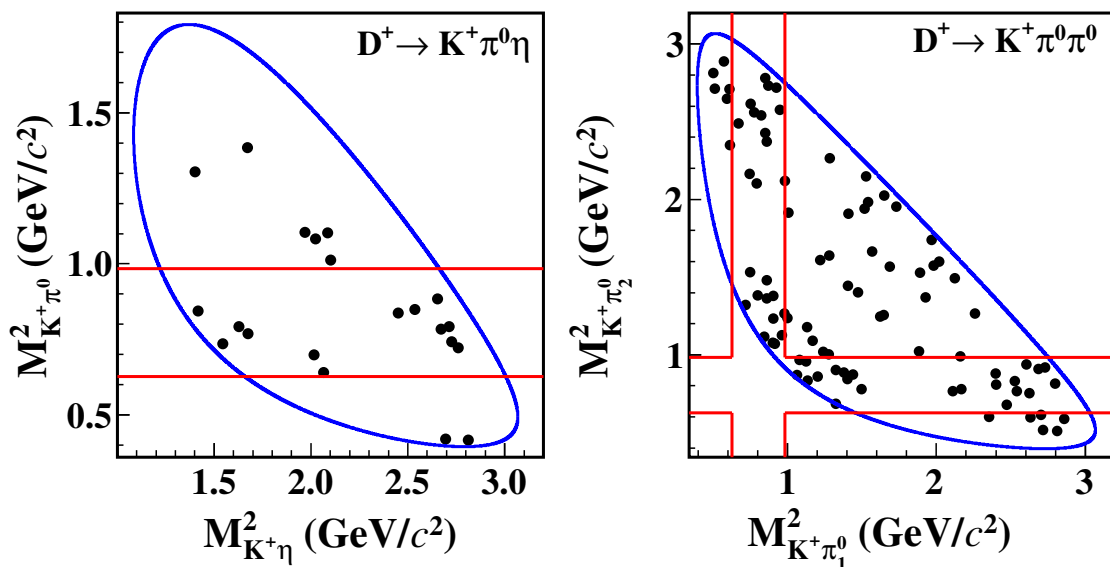


Figure 2. Distributions of (left) $M_{K^+\pi^0}^2$ versus $M_{K^+\eta}^2$ for $D^+ \rightarrow K^+\pi^0\eta$ candidates and (right) $M_{K^+\pi^0}^2$ versus $M_{K^+\pi_1^0}^2$ for $D^+ \rightarrow K^+\pi^0\pi^0$ candidates (two entries per event for symmetrization). In the kinematic region marked in blue, the regions inside and outside the red band are the K^{*+} signal and sideband regions, respectively. The requirement of $|M_{\text{BC}}^{\text{tag}(\text{sig})} - M_{D^+}| < 0.005 \text{ GeV}/c^2$ has been imposed.

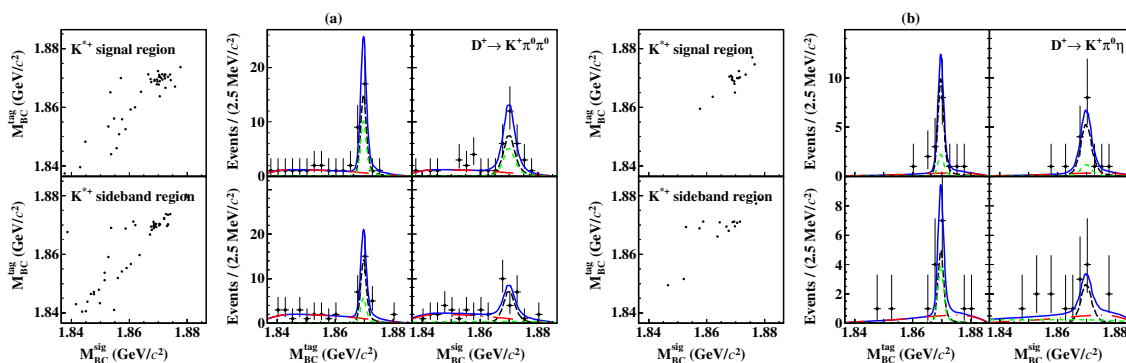


Figure 3. Distributions of (left column) $M_{\text{BC}}^{\text{tag}}$ versus $M_{\text{BC}}^{\text{sig}}$ and the projections on (middle column) $M_{\text{BC}}^{\text{tag}}$ and (right column) $M_{\text{BC}}^{\text{sig}}$ of the constrained 2D fits to the DT candidate events in the K^{*+} signal region (top row) and sideband region (bottom row) for (a) $D^+ \rightarrow K^+\pi^0\pi^0$ and (b) $D^+ \rightarrow K^+\pi^0\eta$. Points with error bars are data. Blue solid curves are the fit results. Black dotted curves are the signal distributions. For the K^{*+} sideband region, green dotted and red dot-long-dashed curves are BKG I and BKG II, respectively. For the K^{*+} signal region, red dot-long-dashed curves are BKG II and green dotted curves are the peaking backgrounds constrained by using the K^{*+} sideband events.

Decay mode	N_{DT}	$\epsilon_{\text{sig}} (\%)$	$\mathcal{B}_{\text{sig}} (\times 10^{-4})$
$D^+ \rightarrow K^+ \pi^0 \pi^0$	42.8 ± 7.2	18.08 ± 0.03	$2.1 \pm 0.4 \pm 0.1$
$D^+ \rightarrow K^+ \pi^0 \eta$	19.2 ± 5.0	20.50 ± 0.03	$2.1 \pm 0.5 \pm 0.1$
$D^+ \rightarrow K^{*+} \pi^0$	$16.6^{+6.6}_{-6.2}$	13.02 ± 0.03	$3.4^{+1.4}_{-1.3} \pm 0.1$
$D^+ \rightarrow K^{*+} \eta$	$10.9^{+4.4}_{-3.8}$	16.60 ± 0.04	$4.4^{+1.8}_{-1.5} \pm 0.2$

Table 2. The DT yields in data (N_{DT}), the signal efficiencies ($\epsilon_{\text{sig}} = \epsilon_{\text{DT}}^i / \epsilon_{\text{ST}}^i$) and the obtained BF. The first and second uncertainties are statistical and systematic, respectively. The efficiencies do not include the BF of π^0 , η and K^{*+} decays. The lower efficiency for $D^+ \rightarrow K^+ \pi^0 \pi^0$ is mainly due to the K_S^0 rejection.

- **ST yields (N_{tag}):** the uncertainty of the total ST D^- yield, which is mainly due to the fit to the $M_{\text{BC}}^{\text{tag}}$ distribution, has been previously estimated to be 0.5% in ref. [31].
- **K^\pm tracking or particle identification (PID):** the efficiencies of tracking and PID of the K^+ are studied with DT $D\bar{D}$ hadronic events. The systematic uncertainty for K^+ tracking and PID is 1.0% for each.
- **π^0 (η) reconstruction:** the efficiency of π^0 reconstruction is investigated using DT $D\bar{D}$ hadronic decay samples of $D^0 \rightarrow K^- \pi^+$, $K^- \pi^+ \pi^+ \pi^-$ versus $\bar{D}^0 \rightarrow K^+ \pi^- \pi^0$, $K_S^0 \pi^0$ [36, 37]. The systematic uncertainty due to π^0 reconstruction is 2.0% per π^0 . Based on the π^0 uncertainty, the systematic uncertainty of η reconstruction is also taken to be 2.0%. The total systematic uncertainty due to $\pi^0 \pi^0$ or $\pi^0 \eta$ reconstruction is obtained to be 4.0% by adding each of them linearly.
- **Quoted BF:** the uncertainties on the quoted BF of $\eta \rightarrow \gamma\gamma$ and $\pi^0 \rightarrow \gamma\gamma$ are 0.5% and 0.03% [13], respectively.
- **2D fit:** the systematic uncertainty of the 2D fit is mainly due to the signal and background shapes. To compensate for the possible data-MC difference of the signal, the MC-simulated signal shapes have been smeared by a Gaussian resolution function with parameters derived from the control sample of $D^+ \rightarrow \pi^+ \pi^0 \pi^0$. Therefore, the systematic uncertainty due to the signal shape is ignored. To consider the uncertainty of center-of-mass energy calibration [38], the endpoint of the ARGUS background function is varied by $\pm 0.2 \text{ MeV}/c^2$. The changes of the BF are assigned as the corresponding systematic uncertainties, which are 0.2% for both $D^+ \rightarrow K^+ \pi^0 \pi^0$ and $D^+ \rightarrow K^+ \pi^0 \eta$, but are negligible for $D^+ \rightarrow K^{*+} \pi^0$ and $D^+ \rightarrow K^{*+} \eta$.
- **$D^+ D^-$ opening angle:** the systematic uncertainty arising from the $D^+ D^-$ opening angle requirement is studied by using the control sample of $D^+ \rightarrow \pi^+ \pi^0 \pi^0$. The difference of the acceptance efficiencies between data and MC simulation, 1.2%, is assigned as the corresponding systematic uncertainty.
- **ΔE^{sig} requirement:** the systematic uncertainty of the ΔE_{sig} requirement is estimated by convolving with one Gaussian resolution function obtained from the control

sample with the ΔE_{sig} distribution of the signal MC events. The change of the DT efficiency is found to be negligible. Therefore, the corresponding systematic uncertainty is neglected.

- **K_S^0 rejection:** the systematic uncertainty due to the K_S^0 rejection is also negligible since the BFs are found to be insensitive to shrinking or enlarging the K_S^0 rejection window by $0.02 \text{ GeV}/c^2$, which is about two standard deviations of the fitted $K_S^0(\rightarrow \pi^0\pi^0)$ resolution, and taking into account correlations of the two signal samples with the nominal and varied K_S^0 signal regions [39].
- **K^{*+} signal region:** the systematic uncertainty of the K^{*+} signal region is studied using DT events from the processes $D^0 \rightarrow K^-\pi^+$ and $K^-\pi^+\pi^0$ versus $\bar{D}^0 \rightarrow K^{*+}(\rightarrow K^+\pi^0)e^-\bar{\nu}_e$. The change of the DT efficiencies after convolving with the obtained Gaussian resolution function with the $M_{K^+\pi^0}$ distributions, 0.1%, is assigned as the associated uncertainty.
- **MC statistics:** the uncertainties of MC statistics are 0.2%, 0.2%, 0.3%, and 0.3% for $D^+ \rightarrow K^+\pi^0\pi^0$, $D^+ \rightarrow K^+\pi^0\eta$, $D^+ \rightarrow K^{*+}\pi^0$, and $D^+ \rightarrow K^{*+}\eta$, respectively.
- **MC modeling:** the systematic uncertainties related to the MC modeling for $D^+ \rightarrow K^+\pi^0\pi^0$ and $D^+ \rightarrow K^+\pi^0\eta$ are estimated by varying $r_{K^{*+}\pi^0(\eta)}$ by $\pm 1\sigma$. The changes of the detection efficiencies are assigned as the corresponding systematic uncertainties, which are 2.1% and 1.6% for $D^+ \rightarrow K^+\pi^0\pi^0$ and $D^+ \rightarrow K^+\pi^0\eta$, respectively.
- **Scale factor of K^{*+} sideband:** the systematic uncertainties due to the scale factors of K^{*+} sideband are examined by varying $f_{K^{*+}\pi^0}$ and $f_{K^{*+}\eta}$ by $\pm 1\sigma$. The changes of the re-measured BFs, 1.4% and 0.5%, are assigned as the systematic uncertainties for $D^+ \rightarrow K^{*+}\pi^0$ and $D^+ \rightarrow K^{*+}\eta$, respectively.
- **Multiplicities of tag and signal sides:** to verify the smallest $|\Delta E|$ selection method, we have examined the multiple candidate rates for the tag and signal sides. Due to limited signal statistics, the signal side is examined with the control sample of $D^+ \rightarrow \pi^+\pi^0\pi^0$, which has similar multiple candidate rates as our signal candidates. The multiple candidate rates of $D^- \rightarrow K^+\pi^-\pi^-$, $D^- \rightarrow K_S^0\pi^-$, $D^- \rightarrow K^+\pi^-\pi^-\pi^0$, and $D^+ \rightarrow \pi^+\pi^0\pi^0$ are about 0.4%, 0.2%, 9.9%, and 1.7% with negligible uncertainties, respectively, for both data and MC simulation. Therefore, the relevant effect is ignored in this analysis.

Adding the above effects in quadrature yields the total systematic uncertainty for each signal process. They are 4.7%, 4.5%, 4.4%, and 4.3% for $D^+ \rightarrow K^+\pi^0\pi^0$, $D^+ \rightarrow K^+\pi^0\eta$, $D^+ \rightarrow K^{*+}\pi^0$, and $D^+ \rightarrow K^{*+}\eta$, respectively. Table 3 summarizes the systematic uncertainties discussed above.

6 Summary

In summary, using 2.93 fb^{-1} of e^+e^- annihilation data [14, 15] taken at $\sqrt{s} = 3.773 \text{ GeV}$, we report the first observations of the DCS decays $D^+ \rightarrow K^+\pi^0\pi^0$ and $D^+ \rightarrow K^+\pi^0\eta$, as well as the first searches for $D^+ \rightarrow K^{*+}\pi^0$ and $D^+ \rightarrow K^{*+}\eta$. It should be noted

Uncertainty	$K^+\pi^0\pi^0$	$K^+\pi^0\eta$	$K^{*+}\pi^0$	$K^{*+}\eta$
N_{tag}	0.5	0.5	0.5	0.5
K^\pm tracking	1.0	1.0	1.0	1.0
K^\pm PID	1.0	1.0	1.0	1.0
$\pi^0(\eta)$ reconstruction	4.0	4.0	4.0	4.0
Quoted BFs	Negligible	0.5	Negligible	0.5
2D fit	0.2	0.2	Negligible	Negligible
D^+D^- opening angle	1.2	1.2	1.2	1.2
ΔE^{sig} requirement	Negligible	Negligible	Negligible	Negligible
K_S^0 rejection	Negligible	Negligible	Negligible	Negligible
K^{*+} signal region	—	—	0.1	0.1
MC statistics	0.2	0.2	0.3	0.3
MC modeling	2.1	1.6	—	—
Scale factor of K^{*+} sideband	—	—	1.4	0.5
Multiplicities of tag and signal sides	Negligible	Negligible	Negligible	Negligible
Total	4.7	4.5	4.4	4.3

Table 3. Systematic uncertainties (%) in the measurements of the BFs.

that the BFs of $D^+ \rightarrow K^{*+}\pi^0(\eta)$ are measured under the assumptions that there is no interference between resonant and non-resonant components, and the non-resonant component is uniformly distributed in the phase space. The obtained BFs are summarized in table 2. We also set an upper limit on the BF of $D^+ \rightarrow K^{*+}\pi^0$ decays of to be 5.4×10^{-4} at the 90% confidence level. Our $D^+ \rightarrow K^{*+}\pi^0$ and $D^+ \rightarrow K^{*+}\eta$ BF results supply important information for more detailed investigations of SU(3)-flavor symmetry breaking effects as well as for the understanding of CP violation phenomena in hadronic decays of charmed mesons. Our measured $\mathcal{B}_{D^+ \rightarrow K^{*+}\pi^0}$ is consistent with the predictions in refs. [1–3], while $\mathcal{B}_{D^+ \rightarrow K^{*+}\eta}$ differs from all predictions by approximately 2σ . With the obtained BFs of $D^+ \rightarrow K^{*+}\pi^0$ and $D^+ \rightarrow K^{*+}\eta$, we set an upper limit on the BF ratio to be $\mathcal{B}_{D^+ \rightarrow K^{*+}\pi^0}/\mathcal{B}_{D^+ \rightarrow K^{*+}\eta} < 1.64$ at the 90% confidence level. Combining our $\mathcal{B}_{D^+ \rightarrow K^+\pi^0\pi^0}$ and $\mathcal{B}_{D^+ \rightarrow K^+\pi^0\eta}$ with $\mathcal{B}_{D^+ \rightarrow K^-\pi^+\pi^+} = (9.38 \pm 0.16)\%$ [13] and $\mathcal{B}(D^+ \rightarrow K_S^0\pi^+\eta) = (1.31 \pm 0.04 \pm 0.03)\%$ [40], we obtain the relative DCS to CF BF ratios $\mathcal{B}_{D^+ \rightarrow K^+\pi^0\pi^0}/\mathcal{B}_{D^+ \rightarrow K^-\pi^+\pi^+} = (2.24 \pm 0.40) \times 10^{-3}$ and $\mathcal{B}_{D^+ \rightarrow K^+\pi^0\eta}/\mathcal{B}_{D^+ \rightarrow \bar{K}^0\pi^+\eta} = (8.01 \pm 1.97) \times 10^{-3}$. They correspond to $(0.77 \pm 0.14) \tan^4 \theta_C$ and $(2.64 \pm 0.68) \tan^4 \theta_C$, respectively. The former ratio is consistent with the naive prediction $\frac{2}{3} \tan^4 \theta_C$, while the latter differs from the naive expectation of $\tan^4 \theta_C$ by 2.4σ . Making use of $\mathcal{B}_{D^+ \rightarrow K^+\pi^+\pi^-} = (4.91 \pm 0.09) \times 10^{-4}$ [13], we determine $\mathcal{B}(D^+ \rightarrow K^+\pi^0\pi^0)/\mathcal{B}(D^+ \rightarrow K^+\pi^+\pi^-) = 0.43 \pm 0.08$, which is consistent with prediction assuming isospin symmetry between these two decays.

Acknowledgments

The authors thank Professors Yu-Kuo Hsiao, Qin Qin, and Fusheng Yu for helpful discussions. The BESIII collaboration thanks the staff of BEPCII and the IHEP computing center for their strong support. This work is supported in part by National Key R&D Program of China under Contracts Nos. 2020YFA0406400 and 2020YFA0406300; National Natural Science Foundation of China (NSFC) under Contracts Nos. 11775230, 11625523, 11635010, 11735014, 11822506, 11835012, 11935015, 11935016, 11935018, 11961141012, 12022510, 12025502, 12035009, 12035013, 12061131003, 12192260, 12192261, 12192262, 12192263, 12192264, 12192265; the Chinese Academy of Sciences (CAS) Large-Scale Scientific Facility Program; Joint Large-Scale Scientific Facility Funds of the NSFC and CAS under Contracts Nos. U1732263, U1832207, U1932102; CAS Key Research Program of Frontier Sciences under Contract No. QYZDJ-SSW-SLH040; the CAS Center for Excellence in Particle Physics (CCEPP); 100 Talents Program of CAS; INPAC and Shanghai Key Laboratory for Particle Physics and Cosmology; ERC under Contract No. 758462; European Union Horizon 2020 research and innovation programme under Contract No. Marie Skłodowska-Curie grant agreement No 894790; German Research Foundation DFG under Contracts Nos. 443159800, Collaborative Research Center CRC 1044, FOR 2359, FOR 2359, GRK 214; Istituto Nazionale di Fisica Nucleare, Italy; Ministry of Development of Turkey under Contract No. DPT2006K-120470; National Science and Technology fund; Olle Engkvist Foundation under Contract No. 200-0605; STFC (United Kingdom); The Knut and Alice Wallenberg Foundation (Sweden) under Contract No. 2016.0157; The Royal Society, U.K. under Contracts Nos. DH140054, DH160214; The Swedish Research Council; U.S. Department of Energy under Contracts Nos. DE-FG02-05ER41374, DE-SC-0012069.

Open Access. This article is distributed under the terms of the Creative Commons Attribution License ([CC-BY 4.0](https://creativecommons.org/licenses/by/4.0/)), which permits any use, distribution and reproduction in any medium, provided the original author(s) and source are credited. SCOAP³ supports the goals of the International Year of Basic Sciences for Sustainable Development.

References

- [1] Y. Fu-Sheng, X.-X. Wang and C.-D. Lü, *Nonleptonic two body decays of charmed mesons*, *Phys. Rev. D* **84** (2011) 074019 [[arXiv:1101.4714](https://arxiv.org/abs/1101.4714)] [[INSPIRE](https://inspirehep.net/literature/94411)].
- [2] Q. Qin, H.-N. Li, C.-D. Lü and F.-S. Yu, *Branching ratios and direct CP asymmetries in $D \rightarrow PV$ decays*, *Phys. Rev. D* **89** (2014) 054006 [[arXiv:1305.7021](https://arxiv.org/abs/1305.7021)] [[INSPIRE](https://inspirehep.net/literature/1114101)].
- [3] H.-Y. Cheng, C.-W. Chiang and A.-L. Kuo, *Global analysis of two-body $D \rightarrow VP$ decays within the framework of flavor symmetry*, *Phys. Rev. D* **93** (2016) 114010 [[arXiv:1604.03761](https://arxiv.org/abs/1604.03761)] [[INSPIRE](https://inspirehep.net/literature/1441101)].
- [4] H.-Y. Cheng and C.-W. Chiang, *Two-body hadronic charmed meson decays*, *Phys. Rev. D* **81** (2010) 074021 [[arXiv:1001.0987](https://arxiv.org/abs/1001.0987)] [[INSPIRE](https://inspirehep.net/literature/85411)].
- [5] W. Kwong and S.P. Rosen, *Minimal breaking of flavor SU(3) in nonleptonic charm decay*, *Phys. Lett. B* **298** (1993) 413 [[INSPIRE](https://inspirehep.net/literature/31111)].

- [6] Y. Grossman and D.J. Robinson, SU(3) *sum rules for charm decay*, *JHEP* **04** (2013) 067 [[arXiv:1211.3361](#)] [[INSPIRE](#)].
- [7] H.-N. Li, C.-D. Lü and F.-S. Yu, *Branching ratios and direct CP asymmetries in $D \rightarrow PP$ decays*, *Phys. Rev. D* **86** (2012) 036012 [[arXiv:1203.3120](#)] [[INSPIRE](#)].
- [8] H.J. Lipkin, *The importance of the K_η and K'_η decay modes in understanding charmed and other meson decays*, *Phys. Rev. Lett.* **46** (1981) 1307 [[INSPIRE](#)].
- [9] N. Cabibbo, *Unitary symmetry and leptonic decays*, *Phys. Rev. Lett.* **10** (1963) 531 [[INSPIRE](#)].
- [10] H.J. Lipkin, *Puzzles in hyperon, charm and beauty physics*, *Nucl. Phys. B Proc. Suppl.* **115** (2003) 117 [[hep-ph/0210166](#)] [[INSPIRE](#)].
- [11] M. Peshkin and J.L. Rosner, *Isospin restrictions on charge distributions in charmed particle decays*, *Nucl. Phys. B* **122** (1977) 144 [[INSPIRE](#)].
- [12] M. Gronau and J.L. Rosner, *D_s inclusive decays*, *Phys. Rev. D* **79** (2009) 074022 [[arXiv:0903.2287](#)] [[INSPIRE](#)].
- [13] PARTICLE DATA GROUP collaboration, *Review of particle physics*, *PTEP* **2020** (2020) 083C01 [[INSPIRE](#)].
- [14] BESIII collaboration, *Measurement of the integrated luminosities of the data taken by BESIII at $\sqrt{s} = 3.650$ and 3.773 GeV*, *Chin. Phys. C* **37** (2013) 123001 [[arXiv:1307.2022](#)] [[INSPIRE](#)].
- [15] BESIII collaboration, *Measurement of the $e^+e^- \rightarrow \pi^+\pi^-$ cross section between 600 and 900 MeV using initial state radiation*, *Phys. Lett. B* **753** (2016) 629 [Erratum *ibid.* **812** (2021) 135982] [[arXiv:1507.08188](#)] [[INSPIRE](#)].
- [16] C. Yu et al., *BEPChII performance and beam dynamics studies on luminosity*, in *Proceedings of the 7th Int. Particle Accelerator Conf.*, **IPAC2016**, Korea (2016).
- [17] BESIII collaboration, *Design and construction of the BESIII detector*, *Nucl. Instrum. Meth. A* **614** (2010) 345 [[arXiv:0911.4960](#)] [[INSPIRE](#)].
- [18] GEANT4 collaboration, *GEANT4 — a simulation toolkit*, *Nucl. Instrum. Meth. A* **506** (2003) 250 [[INSPIRE](#)].
- [19] J. Allison et al., *GEANT4 developments and applications*, *IEEE Trans. Nucl. Sci.* **53** (2006) 270 [[INSPIRE](#)].
- [20] J. Allison et al., *Recent developments in GEANT4*, *Nucl. Instrum. Meth. A* **835** (2016) 186 [[INSPIRE](#)].
- [21] S. Jadach, B.F.L. Ward and Z. Was, *The precision Monte Carlo event generator KK for two fermion final states in e^+e^- collisions*, *Comput. Phys. Commun.* **130** (2000) 260 [[hep-ph/9912214](#)] [[INSPIRE](#)].
- [22] S. Jadach, B.F.L. Ward and Z. Was, *Coherent exclusive exponentiation for precision Monte Carlo calculations*, *Phys. Rev. D* **63** (2001) 113009 [[hep-ph/0006359](#)] [[INSPIRE](#)].
- [23] D.J. Lange, *The EvtGen particle decay simulation package*, *Nucl. Instrum. Meth. A* **462** (2001) 152 [[INSPIRE](#)].
- [24] R.-G. Ping, *Event generators at BESIII*, *Chin. Phys. C* **32** (2008) 599 [[INSPIRE](#)].
- [25] J.C. Chen, G.S. Huang, X.R. Qi, D.H. Zhang and Y.S. Zhu, *Event generator for J/ψ and $\psi(2S)$ decay*, *Phys. Rev. D* **62** (2000) 034003 [[INSPIRE](#)].

- [26] R.-L. Yang, R.-G. Ping and H. Chen, *Tuning and validation of the Lundcharm model with J/ψ decays*, *Chin. Phys. Lett.* **31** (2014) 061301 [[INSPIRE](#)].
- [27] E. Richter-Was, *QED bremsstrahlung in semileptonic B and leptonic τ decays*, *Phys. Lett. B* **303** (1993) 163 [[INSPIRE](#)].
- [28] E. Barberio, B. van Eijk and Z. Was, *PHOTOS: a universal Monte Carlo for QED radiative corrections in decays*, *Comput. Phys. Commun.* **66** (1991) 115 [[INSPIRE](#)].
- [29] P. Golonka and Z. Was, *PHOTOS Monte Carlo: a precision tool for QED corrections in Z and W decays*, *Eur. Phys. J. C* **45** (2006) 97 [[hep-ph/0506026](#)] [[INSPIRE](#)].
- [30] MARK-III collaboration, *Direct measurements of charmed d meson hadronic branching fractions*, *Phys. Rev. Lett.* **56** (1986) 2140 [[INSPIRE](#)].
- [31] BESIII collaboration, *Observation of $D^+ \rightarrow \eta\eta\pi^+$ and improved measurement of $D^{0(+)} \rightarrow \eta\pi^+\pi^{-(0)}$* , *Phys. Rev. D* **101** (2020) 052009 [[arXiv:1912.12411](#)] [[INSPIRE](#)].
- [32] BESIII collaboration, *Observation of the doubly Cabibbo-suppressed decay $D^+ \rightarrow K^+\pi^+\pi^-\pi^0$ and evidence for $D^+ \rightarrow K^+\omega$* , *Phys. Rev. Lett.* **125** (2020) 141802 [[arXiv:2007.07674](#)] [[INSPIRE](#)].
- [33] CLEO collaboration, *Measurement of absolute hadronic branching fractions of D mesons and $e^+e^- \rightarrow D\bar{D}$ cross-sections at the $\psi(3770)$* , *Phys. Rev. D* **76** (2007) 112001 [[arXiv:0709.3783](#)] [[INSPIRE](#)].
- [34] BESIII collaboration, *Measurement of the $D \rightarrow K^-\pi^+$ strong phase difference in $\psi(3770) \rightarrow D^0\bar{D}^0$* , *Phys. Lett. B* **734** (2014) 227 [[arXiv:1404.4691](#)] [[INSPIRE](#)].
- [35] K. Stenson, *A more exact solution for incorporating multiplicative systematic uncertainties in branching ratio limits*, [physics/0605236](#) [[INSPIRE](#)].
- [36] BESIII collaboration, *Improved measurement of the absolute branching fraction of $D^+ \rightarrow \bar{K}^0\mu^+\nu_\mu$* , *Eur. Phys. J. C* **76** (2016) 369 [[arXiv:1605.00068](#)] [[INSPIRE](#)].
- [37] BESIII collaboration, *Measurement of the absolute branching fraction of $D^+ \rightarrow \bar{K}^0e^+\nu_e$ via $\bar{K}^0 \rightarrow \pi^0\pi^0$* , *Chin. Phys. C* **40** (2016) 113001 [[arXiv:1605.00208](#)] [[INSPIRE](#)].
- [38] B. Wang, L.Y. Dong and X.D. Ruan, *BEPCII center-of-mass beam energy calibration for $\psi(3770)$ data* (in Chinese), *Nucl. Electron. Detect. Technol.* **33** (2013) 2.
- [39] R. Barlow, *Systematic errors: facts and fictions*, in *Conference on advanced statistical techniques in particle physics*, (2002), p. 134 [[hep-ex/0207026](#)] [[INSPIRE](#)].
- [40] BESIII collaboration, *Measurements of absolute branching fractions of fourteen exclusive hadronic D decays to η* , *Phys. Rev. Lett.* **124** (2020) 241803 [[arXiv:2004.13910](#)] [[INSPIRE](#)].

The BESIII collaboration

M. Ablikim¹, M. N. Achasov^{10,b}, P. Adlarson⁶⁸, S. Ahmed¹⁴, M. Albrecht⁴, R. Aliberti²⁸, A. Amoroso^{67A,67C}, M. R. An³², Q. An^{64,50}, X. H. Bai⁵⁸, Y. Bai⁴⁹, O. Bakina²⁹, R. Baldini Ferroli^{23A}, I. Balossino^{24A}, Y. Ban^{39,h}, K. Begzsuren²⁶, N. Berger²⁸, M. Bertani^{23A}, D. Bettoni^{24A}, F. Bianchi^{67A,67C}, J. Bloms⁶¹, A. Bortone^{67A,67C}, I. Boyko²⁹, R. A. Briere⁵, A. Brueggemann⁶¹, H. Cai⁶⁹, X. Cai^{1,50}, A. Calcaterra^{23A}, G. F. Cao^{1,55}, N. Cao^{1,55}, S. A. Cetin^{54A}, J. F. Chang^{1,50}, W. L. Chang^{1,55}, G. Chelkov^{29,a}, G. Chen¹, H. S. Chen^{1,55}, M. L. Chen^{1,50}, S. J. Chen³⁵, X. R. Chen²⁵, Y. B. Chen^{1,50}, Z. J. Chen^{20,i}, W. S. Cheng^{67C}, G. Cibinetto^{24A}, F. Cossio^{67C}, J. J. Cui⁴², H. L. Dai^{1,50}, J. P. Dai⁷¹, A. Dbeysi¹⁴, R. E. de Boer⁴, D. Dedovich²⁹, Z. Y. Deng¹, A. Denig²⁸, I. Denysenko²⁹, M. Destefanis^{67A,67C}, F. De Mori^{67A,67C}, Y. Ding³³, J. Dong^{1,50}, L. Y. Dong^{1,55}, M. Y. Dong^{1,50,55}, X. Dong⁶⁹, S. X. Du⁷³, Y. L. Fan⁶⁹, J. Fang^{1,50}, S. S. Fang^{1,55}, Y. Fang¹, R. Farinelli^{24A}, L. Fava^{67B,67C}, F. Feldbauer⁴, G. Felici^{23A}, C. Q. Feng^{64,50}, J. H. Feng⁵¹, M. Fritsch⁴, C. D. Fu¹, Y. N. Gao^{39,h}, Yang Gao^{64,50}, I. Garzia^{24A,24B}, P. T. Ge⁶⁹, C. Geng⁵¹, E. M. Gersabeck⁵⁹, A. Gilman⁶², K. Goetzen¹¹, L. Gong³³, W. X. Gong^{1,50}, W. Gradl²⁸, M. Greco^{67A,67C}, L. M. Gu³⁵, M. H. Gu^{1,50}, C. Y. Guan^{1,55}, A. Q. Guo²⁵, A. Q. Guo²², L. B. Guo³⁴, R. P. Guo⁴¹, Y. P. Guo^{9,g}, A. Guskov^{29,a}, T. T. Han⁴², W. Y. Han³², X. Q. Hao¹⁵, F. A. Harris⁵⁷, K. L. He^{1,55}, F. H. Heinsius⁴, C. H. Heinz²⁸, Y. K. Heng^{1,50,55}, C. Herold⁵², M. Himmelreich^{11,e}, T. Holtmann⁴, G. Y. Hou^{1,55}, Y. R. Hou⁵⁵, Z. L. Hou¹, H. M. Hu^{1,55}, J. F. Hu^{48,j}, T. Hu^{1,50,55}, Y. Hu¹, G. S. Huang^{64,50}, L. Q. Huang⁶⁵, X. T. Huang⁴², Y. P. Huang¹, Z. Huang^{39,h}, T. Hussain⁶⁶, N. Hüsken^{22,28}, W. Imoehl²², M. Irshad^{64,50}, S. Jaeger⁴, S. Janchiv²⁶, Q. Ji¹, Q. P. Ji¹⁵, X. B. Ji^{1,55}, X. L. Ji^{1,50}, Y. Y. Ji⁴², H. B. Jiang⁴², X. S. Jiang^{1,50,55}, J. B. Jiao⁴², Z. Jiao¹⁸, S. Jin³⁵, Y. Jin⁵⁸, M. Q. Jing^{1,55}, T. Johansson⁶⁸, N. Kalantar-Nayestanaki⁵⁶, X. S. Kang³³, R. Kappert⁵⁶, M. Kavatsyuk⁵⁶, B. C. Ke⁷³, I. K. Keshk⁴, A. Khoukaz⁶¹, P. Kiese²⁸, R. Kiuchi¹, R. Kliemt¹¹, L. Koch³⁰, O. B. Kolcu^{54A}, B. Kopf⁴, M. Kuemmel⁴, M. Kuessner⁴, A. Kupsc^{37,68}, W. Kühn³⁰, J. J. Lane⁵⁹, J. S. Lange³⁰, P. Larin¹⁴, A. Lavanaia²¹, L. Lavezzi^{67A,67C}, Z. H. Lei^{64,50}, H. Leithoff²⁸, M. Lellmann²⁸, T. Lenz²⁸, C. Li⁴⁰, C. H. Li³², Cheng Li^{64,50}, D. M. Li⁷³, F. Li^{1,50}, G. Li¹, H. Li^{64,50}, H. Li⁴⁴, H. B. Li^{1,55}, H. J. Li¹⁵, H. N. Li^{48,j}, J. L. Li⁴², J. Q. Li⁴, J. S. Li⁵¹, Ke Li¹, L. K. Li¹, Lei Li³, P. R. Li^{31,k,l}, S. Y. Li⁵³, T. Li⁴², W. D. Li^{1,55}, W. G. Li¹, X. H. Li^{64,50}, X. L. Li⁴², Xiaoyu Li^{1,55}, Z. Y. Li⁵¹, H. Liang²⁷, H. Liang^{1,55}, H. Liang^{64,50}, Y. F. Liang⁴⁶, Y. T. Liang²⁵, G. R. Liao¹², J. Libby²¹, A. Limphirat⁵², C. X. Lin⁵¹, D. X. Lin²⁵, T. Lin¹, B. J. Liu¹, C. X. Liu¹, D. Liu^{14,64}, F. H. Liu⁴⁵, Fang Liu¹, Feng Liu⁶, G. M. Liu^{48,j}, H. M. Liu^{1,55}, Huanhuan Liu¹, Huihui Liu¹⁶, J. B. Liu^{64,50}, J. L. Liu⁶⁵, J. Y. Liu^{1,55}, K. Liu¹, K. Y. Liu³³, Ke Liu¹⁷, L. Liu^{64,50}, M. H. Liu^{9,g}, P. L. Liu¹, Q. Liu⁵⁵, Q. Liu⁶⁹, S. B. Liu^{64,50}, T. Liu^{9,g}, W. M. Liu^{64,50}, X. Liu^{31,k,l}, Y. Liu^{31,k,l}, Y. B. Liu³⁶, Z. A. Liu^{1,50,55}, Z. Q. Liu⁴², X. C. Lou^{1,50,55}, F. X. Lu⁵¹, H. J. Lu¹⁸, J. G. Lu^{1,50}, X. L. Lu¹, Y. Lu¹, Y. P. Lu^{1,50}, C. L. Luo³⁴, M. X. Luo⁷², T. Luo^{9,g}, X. L. Luo^{1,50}, X. R. Lyu⁵⁵, F. C. Ma³³, H. L. Ma¹, L. L. Ma⁴², M. M. Ma^{1,55}, Q. M. Ma¹, R. Q. Ma^{1,55}, R. T. Ma⁵⁵, X. Y. Ma^{1,50}, Y. Ma^{39,h}, F. E. Maas¹⁴, M. Maggiora^{67A,67C}, S. Maldaner⁴, S. Malde⁶², Q. A. Malik⁶⁶, A. Mangoni^{23B}, Y. J. Mao^{39,h}, Z. P. Mao¹, S. Marcello^{67A,67C}, Z. X. Meng⁵⁸, J. G. Messchendorp^{56,d}, G. Mezzadri^{24A}, T. J. Min³⁵, R. E. Mitchell²², X. H. Mo^{1,50,55}, N. Yu. Muchnoi^{10,b}, H. Muramatsu⁶⁰, S. Nakhoul^{11,e}, Y. Nefedov²⁹, F. Nerling^{11,e}, I. B. Nikolaev^{10,b}, Z. Ning^{1,50}, S. Nisar^{8,m}, S. L. Olsen⁵⁵, Q. Ouyang^{1,50,55}, S. Pacetti^{23B,23C}, X. Pan^{9,g}, Y. Pan⁵⁹, A. Pathak¹, A. Pathak²⁷, P. Patteri^{23A}, M. Pelizaeus⁴, H. P. Peng^{64,50}, K. Peters^{11,e}, J. Pettersson⁶⁸, J. L. Ping³⁴, R. G. Ping^{1,55}, S. Pogodin²⁹, R. Poling⁶⁰, V. Prasad^{64,50}, H. Qi^{64,50}, H. R. Qi⁵³, M. Qi³⁵, T. Y. Qi^{9,g}, S. Qian^{1,50}, W. B. Qian⁵⁵, Z. Qian⁵¹, C. F. Qiao⁵⁵, J. J. Qin⁶⁵, L. Q. Qin¹², X. P. Qin^{9,g}, X. S. Qin⁴², Z. H. Qin^{1,50}, J. F. Qiu¹, S. Q. Qu⁵³, K. H. Rashid⁶⁶, K. Ravindran²¹,

C. F. Redmer²⁸, A. Rivetti^{67C}, V. Rodin⁵⁶, M. Rolo^{67C}, G. Rong^{1,55}, Ch. Rosner¹⁴, M. Rump⁶¹, H. S. Sang⁶⁴, A. Sarantsev^{29,c}, Y. Schelhaas²⁸, C. Schnier⁴, K. Schoenning⁶⁸, M. Scodeggio^{24A,24B}, W. Shan¹⁹, X. Y. Shan^{64,50}, J. F. Shanguan⁴⁷, M. Shao^{64,50}, C. P. Shen^{9,g}, H. F. Shen^{1,55}, X. Y. Shen^{1,55}, H. C. Shi^{64,50}, R. S. Shi^{1,55}, X. Shi^{1,50}, X. D Shi^{64,50}, J. J. Song¹⁵, W. M. Song^{27,1}, Y. X. Song^{39,h}, S. Sosio^{67A,67C}, S. Spataro^{67A,67C}, K. X. Su⁶⁹, P. P. Su⁴⁷, G. X. Sun¹, H. K. Sun¹, J. F. Sun¹⁵, L. Sun⁶⁹, S. S. Sun^{1,55}, T. Sun^{1,55}, W. Y. Sun²⁷, X Sun^{20,i}, Y. J. Sun^{64,50}, Y. Z. Sun¹, Z. T. Sun⁴², Y. H. Tan⁶⁹, Y. X. Tan^{64,50}, C. J. Tang⁴⁶, G. Y. Tang¹, J. Tang⁵¹, J. X. Teng^{64,50}, V. Thoren⁶⁸, W. H. Tian⁴⁴, Y. T. Tian²⁵, I. Uman^{54B}, B. Wang¹, C. W. Wang³⁵, D. Y. Wang^{39,h}, H. J. Wang^{31,k,l}, H. P. Wang^{1,55}, K. Wang^{1,50}, L. L. Wang¹, M. Wang⁴², M. Z. Wang^{39,h}, Meng Wang^{1,55}, S. Wang^{9,g}, W. Wang⁵¹, W. H. Wang⁶⁹, W. P. Wang^{64,50}, X. Wang^{39,h}, X. F. Wang^{31,k,l}, X. L. Wang^{9,g}, Y. D. Wang³⁸, Y. F. Wang^{1,50,55}, Y. Q. Wang¹, Y. Y. Wang^{31,k,l}, Ying Wang⁵¹, Z. Wang^{1,50}, Z. Y. Wang¹, Ziyi Wang⁵⁵, D. H. Wei¹², F. Weidner⁶¹, S. P. Wen¹, D. J. White⁵⁹, U. Wiedner⁴, G. Wilkinson⁶², M. Wolke⁶⁸, L. Wollenberg⁴, J. F. Wu^{1,55}, L. H. Wu¹, L. J. Wu^{1,55}, X. Wu^{9,g}, X. H. Wu²⁷, Y. Wu⁶⁴, Z. Wu^{1,50}, L. Xia^{64,50}, T. Xiang^{39,h}, H. Xiao^{9,g}, S. Y. Xiao¹, Z. J. Xiao³⁴, X. H. Xie^{39,h}, Y. G. Xie^{1,50}, Y. H. Xie⁶, Z. P. Xie^{64,50}, T. Y. Xing^{1,55}, C. J. Xu⁵¹, G. F. Xu¹, Q. J. Xu¹³, S. Y. Xu⁶³, X. P. Xu⁴⁷, Y. C. Xu⁵⁵, F. Yan^{9,g}, L. Yan^{9,g}, W. B. Yan^{64,50}, W. C. Yan⁷³, H. J. Yang^{43,f}, H. X. Yang¹, L. Yang⁴⁴, S. L. Yang⁵⁵, Yifan Yang^{1,55}, Zhi Yang²⁵, M. Ye^{1,50}, M. H. Ye⁷, J. H. Yin¹, Z. Y. You⁵¹, B. X. Yu^{1,50,55}, C. X. Yu³⁶, G. Yu^{1,55}, J. S. Yu^{20,i}, T. Yu⁶⁵, C. Z. Yuan^{1,55}, L. Yuan², X. Q. Yuan^{39,h}, Y. Yuan^{1,55}, Z. Y. Yuan⁵¹, C. X. Yue³², A. A. Zafar⁶⁶, X. Zeng⁶, Y. Zeng^{20,i}, A. Q. Zhang¹, B. X. Zhang¹, G. Y. Zhang¹⁵, H. Zhang⁶⁴, H. H. Zhang²⁷, H. H. Zhang⁵¹, H. Y. Zhang^{1,50}, J. L. Zhang⁷⁰, J. Q. Zhang³⁴, J. W. Zhang^{1,50,55}, J. Y. Zhang¹, J. Z. Zhang^{1,55}, Jianyu Zhang^{1,55}, Jiawei Zhang^{1,55}, L. M. Zhang⁵³, L. Q. Zhang⁵¹, Lei Zhang³⁵, S. F. Zhang³⁵, Shulei Zhang^{20,i}, X. D. Zhang³⁸, X. Y. Zhang⁴², Y. Zhang⁶², Y. T. Zhang⁷³, Y. H. Zhang^{1,50}, Yan Zhang^{64,50}, Yao Zhang¹, Z. Y. Zhang⁶⁹, G. Zhao¹, J. Zhao³², J. Y. Zhao^{1,55}, J. Z. Zhao^{1,50}, Lei Zhao^{64,50}, Ling Zhao¹, M. G. Zhao³⁶, Q. Zhao¹, S. J. Zhao⁷³, Y. B. Zhao^{1,50}, Y. X. Zhao²⁵, Z. G. Zhao^{64,50}, A. Zhemchugov^{29,a}, B. Zheng⁶⁵, J. P. Zheng^{1,50}, Y. H. Zheng⁵⁵, B. Zhong³⁴, C. Zhong⁶⁵, L. P. Zhou^{1,55}, X. Zhou⁶⁹, X. K. Zhou⁵⁵, X. R. Zhou^{64,50}, X. Y. Zhou³², J. Zhu³⁶, K. Zhu¹, K. J. Zhu^{1,50,55}, S. H. Zhu⁶³, T. J. Zhu⁷⁰, W. J. Zhu^{9,g}, W. J. Zhu³⁶, Y. C. Zhu^{64,50}, Z. A. Zhu^{1,55}, B. S. Zou¹, J. H. Zou¹

¹ Institute of High Energy Physics, Beijing 100049, People's Republic of China

² Beihang University, Beijing 100191, People's Republic of China

³ Beijing Institute of Petrochemical Technology, Beijing 102617, People's Republic of China

⁴ Bochum Ruhr-University, D-44780 Bochum, Germany

⁵ Carnegie Mellon University, Pittsburgh, Pennsylvania 15213, U.S.A.

⁶ Central China Normal University, Wuhan 430079, People's Republic of China

⁷ China Center of Advanced Science and Technology, Beijing 100190, People's Republic of China

⁸ COMSATS University Islamabad, Lahore Campus, Defence Road, Off Raiwind Road, 54000 Lahore, Pakistan

⁹ Fudan University, Shanghai 200433, People's Republic of China

¹⁰ G.I. Budker Institute of Nuclear Physics SB RAS (BINP), Novosibirsk 630090, Russia

¹¹ GSI Helmholtzcentre for Heavy Ion Research GmbH, D-64291 Darmstadt, Germany

¹² Guangxi Normal University, Guilin 541004, People's Republic of China

¹³ Hangzhou Normal University, Hangzhou 310036, People's Republic of China

¹⁴ Helmholtz Institute Mainz, Staudinger Weg 18, D-55099 Mainz, Germany

¹⁵ Henan Normal University, Xinxiang 453007, People's Republic of China

¹⁶ Henan University of Science and Technology, Luoyang 471003, People's Republic of China

¹⁷ Henan University of Technology, Zhengzhou 450001, People's Republic of China

¹⁸ Huangshan College, Huangshan 245000, People's Republic of China

- ¹⁹ Hunan Normal University, Changsha 410081, People's Republic of China
- ²⁰ Hunan University, Changsha 410082, People's Republic of China
- ²¹ Indian Institute of Technology Madras, Chennai 600036, India
- ²² Indiana University, Bloomington, Indiana 47405, U.S.A.
- ²³ INFN Laboratori Nazionali di Frascati, (A)INFN Laboratori Nazionali di Frascati, I-00044, Frascati, Italy; (B)INFN Sezione di Perugia, I-06100, Perugia, Italy; (C)University of Perugia, I-06100, Perugia, Italy
- ²⁴ INFN Sezione di Ferrara, (A)INFN Sezione di Ferrara, I-44122, Ferrara, Italy; (B)University of Ferrara, I-44122, Ferrara, Italy
- ²⁵ Institute of Modern Physics, Lanzhou 730000, People's Republic of China
- ²⁶ Institute of Physics and Technology, Peace Ave. 54B, Ulaanbaatar 13330, Mongolia
- ²⁷ Jilin University, Changchun 130012, People's Republic of China
- ²⁸ Johannes Gutenberg University of Mainz, Johann-Joachim-Becher-Weg 45, D-55099 Mainz, Germany
- ²⁹ Joint Institute for Nuclear Research, 141980 Dubna, Moscow region, Russia
- ³⁰ Justus-Liebig-Universitaet Giessen, II. Physikalisches Institut, Heinrich-Buff-Ring 16, D-35392 Giessen, Germany
- ³¹ Lanzhou University, Lanzhou 730000, People's Republic of China
- ³² Liaoning Normal University, Dalian 116029, People's Republic of China
- ³³ Liaoning University, Shenyang 110036, People's Republic of China
- ³⁴ Nanjing Normal University, Nanjing 210023, People's Republic of China
- ³⁵ Nanjing University, Nanjing 210093, People's Republic of China
- ³⁶ Nankai University, Tianjin 300071, People's Republic of China
- ³⁷ National Centre for Nuclear Research, Warsaw 02-093, Poland
- ³⁸ North China Electric Power University, Beijing 102206, People's Republic of China
- ³⁹ Peking University, Beijing 100871, People's Republic of China
- ⁴⁰ Qufu Normal University, Qufu 273165, People's Republic of China
- ⁴¹ Shandong Normal University, Jinan 250014, People's Republic of China
- ⁴² Shandong University, Jinan 250100, People's Republic of China
- ⁴³ Shanghai Jiao Tong University, Shanghai 200240, People's Republic of China
- ⁴⁴ Shanxi Normal University, Linfen 041004, People's Republic of China
- ⁴⁵ Shanxi University, Taiyuan 030006, People's Republic of China
- ⁴⁶ Sichuan University, Chengdu 610064, People's Republic of China
- ⁴⁷ Soochow University, Suzhou 215006, People's Republic of China
- ⁴⁸ South China Normal University, Guangzhou 510006, People's Republic of China
- ⁴⁹ Southeast University, Nanjing 211100, People's Republic of China
- ⁵⁰ State Key Laboratory of Particle Detection and Electronics, Beijing 100049, Hefei 230026, People's Republic of China
- ⁵¹ Sun Yat-Sen University, Guangzhou 510275, People's Republic of China
- ⁵² Suranaree University of Technology, University Avenue 111, Nakhon Ratchasima 30000, Thailand
- ⁵³ Tsinghua University, Beijing 100084, People's Republic of China
- ⁵⁴ Turkish Accelerator Center Particle Factory Group, (A)Istinye University, 34010, Istanbul, Turkey; (B)Near East University, Nicosia, North Cyprus, Mersin 10, Turkey
- ⁵⁵ University of Chinese Academy of Sciences, Beijing 100049, People's Republic of China
- ⁵⁶ University of Groningen, NL-9747 AA Groningen, The Netherlands
- ⁵⁷ University of Hawaii, Honolulu, Hawaii 96822, U.S.A.
- ⁵⁸ University of Jinan, Jinan 250022, People's Republic of China
- ⁵⁹ University of Manchester, Oxford Road, Manchester, M13 9PL, United Kingdom
- ⁶⁰ University of Minnesota, Minneapolis, Minnesota 55455, U.S.A.
- ⁶¹ University of Muenster, Wilhelm-Klemm-Str. 9, 48149 Muenster, Germany
- ⁶² University of Oxford, Keble Rd, Oxford, U.K. OX13RH
- ⁶³ University of Science and Technology Liaoning, Anshan 114051, People's Republic of China

- ⁶⁴ *University of Science and Technology of China, Hefei 230026, People’s Republic of China*
- ⁶⁵ *University of South China, Hengyang 421001, People’s Republic of China*
- ⁶⁶ *University of the Punjab, Lahore-54590, Pakistan*
- ⁶⁷ *University of Turin and INFN, (A)University of Turin, I-10125, Turin, Italy; (B)University of Eastern Piedmont, I-15121, Alessandria, Italy; (C)INFN, I-10125, Turin, Italy*
- ⁶⁸ *Uppsala University, Box 516, SE-75120 Uppsala, Sweden*
- ⁶⁹ *Wuhan University, Wuhan 430072, People’s Republic of China*
- ⁷⁰ *Xinyang Normal University, Xinyang 464000, People’s Republic of China*
- ⁷¹ *Yunnan University, Kunming 650500, People’s Republic of China*
- ⁷² *Zhejiang University, Hangzhou 310027, People’s Republic of China*
- ⁷³ *Zhengzhou University, Zhengzhou 450001, People’s Republic of China*
- ^a *Also at the Moscow Institute of Physics and Technology, Moscow 141700, Russia*
- ^b *Also at the Novosibirsk State University, Novosibirsk, 630090, Russia*
- ^c *Also at the NRC “Kurchatov Institute”, PNPI, 188300, Gatchina, Russia*
- ^d *Currently at Istanbul Arel University, 34295 Istanbul, Turkey*
- ^e *Also at Goethe University Frankfurt, 60323 Frankfurt am Main, Germany*
- ^f *Also at Key Laboratory for Particle Physics, Astrophysics and Cosmology, Ministry of Education; Shanghai Key Laboratory for Particle Physics and Cosmology; Institute of Nuclear and Particle Physics, Shanghai 200240, People’s Republic of China*
- ^g *Also at Key Laboratory of Nuclear Physics and Ion-beam Application (MOE) and Institute of Modern Physics, Fudan University, Shanghai 200443, People’s Republic of China*
- ^h *Also at State Key Laboratory of Nuclear Physics and Technology, Peking University, Beijing 100871, People’s Republic of China*
- ⁱ *Also at School of Physics and Electronics, Hunan University, Changsha 410082, China*
- ^j *Also at Guangdong Provincial Key Laboratory of Nuclear Science, Institute of Quantum Matter, South China Normal University, Guangzhou 510006, China*
- ^k *Also at Frontiers Science Center for Rare Isotopes, Lanzhou University, Lanzhou 730000, People’s Republic of China*
- ^l *Also at Lanzhou Center for Theoretical Physics, Lanzhou University, Lanzhou 730000, People’s Republic of China*
- ^m *Also at the Department of Mathematical Sciences, IBA, Karachi, Pakistan*